Chemical Physics Letters 667 (2017) 351–356

Contents lists available at ScienceDirect

Chemical Physics Letters

journal homepage: www.elsevier.com/locate/cplett

Research paper

Facile and low-cost fabrication of Ag-Cu substrates via replacement reaction for highly sensitive SERS applications

Litao Hu [a], Yan Jun Liu [b,*], Shicai Xu [c], Zhe Li [a], Jia Guo [a], Saisai Gao [a], Zhengyi Lu [a], Haipeng Si [d], Shouzhen Jiang [a,*], Shuyun Wang [a]

[a] School of Physics and Electronics, Shandong Normal University, Jinan 250014, China
[b] Department of Electrical and Electronic Engineering, Southern University of Science and Technology, Shenzhen 518055, China
[c] Shandong Provincial Key Laboratory of Biophysics, College of Physics and Electronic Information, Dezhou University, Dezhou 253023, China
[d] Department of Orthopaedics, Qilu Hospital, Shandong University, Jinan 250012, China

ARTICLE INFO

Article history:
Received 25 September 2016
In final form 11 November 2016
Available online 12 November 2016

ABSTRACT

In this work, we demonstrated facile and low-cost fabrication of highly sensitive SERS substrates via replacement reaction by immersing Cu foils into a $AgNO_3$ solution. Different morphologies of Ag nanostructures were observed on the substrate surface by controlling the reaction time. The growth mechanism of Ag nanostructures on the Cu substrates was also analyzed based on the nanostructure evolution. The Ag-Cu substrates showed optimum SERS enhancement at certain reaction time, and the minimum detected concentration of Rhodamine 6G is as low as 10^{-13} M. The easy and low-cost fabrication makes the Ag-Cu SERS substrates promising for rapid, sensitive detection of targeted analytes, such as biomolecules, pollutants, and explosives in the environment.

1. Introduction

Surface enhanced Raman spectroscopy (SERS) has been a powerful technique that allows for highly sensitive detection of analytes with extremely low concentration since its discovery in the 1970s [1–4]. Due to its capability of label-free analysis, SERS has been applied to sensing of various analytes in different fields, such as, metabolites, disease markers, hazardous pollutants, illegal drugs, and explosives in biomedicine, food quality control, environmental monitoring, and security applications [5–11]. However, the enhancement effect of SERS has been under debate between two main mechanisms, i.e., chemical and electromagnetic enhancement, which are supported by formation of charge-transfer complexes and excitation of surface plasmons, respectively. In many reports, the two mechanisms have been proven to be coupled together to collectively contribute the final SERS results [12,13]. Recent results have shown that SERS enhancement occurs even when an excited molecule is relatively far apart from the surface with excitation of surface plasmons [14], providing strong support for the electromagnetic enhancement. Surface plasmons are the light coupled coherent oscillations of free electrons confined at the interfaces of nanostructured metals and dielectric materials [15–17]. With their capability of concentrating and transporting light at the nanoscale, the electromagnetic fields can be exponentially enhanced. This enhancement underpins SERS for high-sensitivity chemical and biochemical analyses. The high sensitivity of SERS can even enable single-molecule detection [18,19]. It has been reported that various metallic nanostructures like Au, Ag and Cu as a SERS substrate have superior Raman enhancement effect [20–22]. Enormous electromagnetic enhancement with tunable plasmonic properties will be formed around the nanoparticles (hot spots) [23]. However, for a success of a SERS sensor, the ease and low-cost substrate fabrication and the highly sensitive, chemically/mechanically stable SERS performance will play a determining role. To this end, a large amount of SERS substrates with various metallic nanostructures and predictable optical response have been heavily investigated [24–27]. Current fabrication methods for SERS substrate include photochemical reactions, self-assembly, nanolithography, and template techniques, etc. These methods are often high-cost and time-consuming. Development of facile and low-cost fabrication is therefore highly desired [28]. From our viewpoint, the fabrication method of galvanic replacement could be one of best options. Galvanic replacement offers a particularly effective approach due to its abilities to control the size and shape of nanoparticles. Recently, dendritic silver nanostructures have been successfully grown via galvanic replacement. Such dendritic nanostructures provide a large number of "hot spots" at the end of branches or the junctions of adjacent Ag branches, which therefore can greatly enhance the

* Corresponding authors.
E-mail addresses: yjliu@sustc.edu.cn (Y.J. Liu), jiang_sz@126.com (S. Jiang).

http://dx.doi.org/10.1016/j.cplett.2016.11.022
0009-2614/

SERS sensitivity. Chan et al. demonstrated ultrastable SERS substrates of Ag dendritic nanostructures coated with silica nanofilm [29]. Liu and Hao fabricated flexible 3D silver dendrite-integrated AAO membrane via electrochemical deposition as effective three-dimensional SERS substrates [30]. Maboudian and coworkers found that Au-coated Ag dendrites as SERS substrates have greatly improved chemical stability and lifetime [31]. However, all the above studies ignore the early growth stage of dendritic silver nanostructures, and the enhancement effect at different growth stages has not been well investigated.

In addition, the growth mechanism of dendritic silver nanostructures is still under debate, it has been widely accepted that formation of this nanostructures results from combined growth mechanisms of Ostwald ripening (OR) and oriented attachment (OA). OR is an important mechanism of crystal growth, in which the small crystallites have a tendency to condense on the surface of the large crystallites, because the higher surface free energy of small crystallites makes them less stable with respect to dissolution in the solvent than large crystallites [32]. As the growth time increases, the surface of crystallite become smooth due to the OR effect [33]. OA is also another significant mechanism in the growth of several nanomaterials. It may occur by collisions of aligned nanocrystals in suspension or rotation of misaligned nanoparticles in contact towards low-energy interface configurations. The anisotropic alignment is attained by restricting the attachment process in some crystallographic directions [34,35]. We will combine these two growth mechanisms to describe the basic structural evolution of our Ag nanostructure system.

In this work, we demonstrate facile and low-cost fabrication of highly sensitive SERS substrates via galvanic replacement reaction by immersing Cu foils into an aqueous $AgNO_3$ solution. Different morphologies of Ag nanostructures can be observed on the substrate surface by controlling the reaction time. The formation mechanism of Ag nanostructures is also analyzed based on the nanostructure evolution. The morphology-dependent SERS effect is tested. The experimental results show that such Ag-Cu substrates are promising for rapid, sensitive SERS detection of various analytes.

2. Experimental

The Cu foils were cut into pieces of 1 cm × 1.5 cm and cleaned sequentially with acetone, ethanol and deionized (DI) water to remove any organic impurities. To obtain fresh Cu surfaces, the cleaned Cu foils were immersed in 1% diluted sulfuric acid to remove surface oxides and then thoroughly rinsed with DI water. The pretreated Cu foils were immersed into an aqueous solution of $AgNO_3$ and the Ag nanostructures were deposited on the Cu foils by the galvanic replacement reaction. Ag ions in the solution were reduced by Cu atoms at the surface of the Cu foil. Continuous reduction of Ag ions by Cu atoms required electron-transfer from the underlying Cu atoms, and the deposition of Ag atoms on Cu surface took place to form Ag nanostructures. In out experiment,

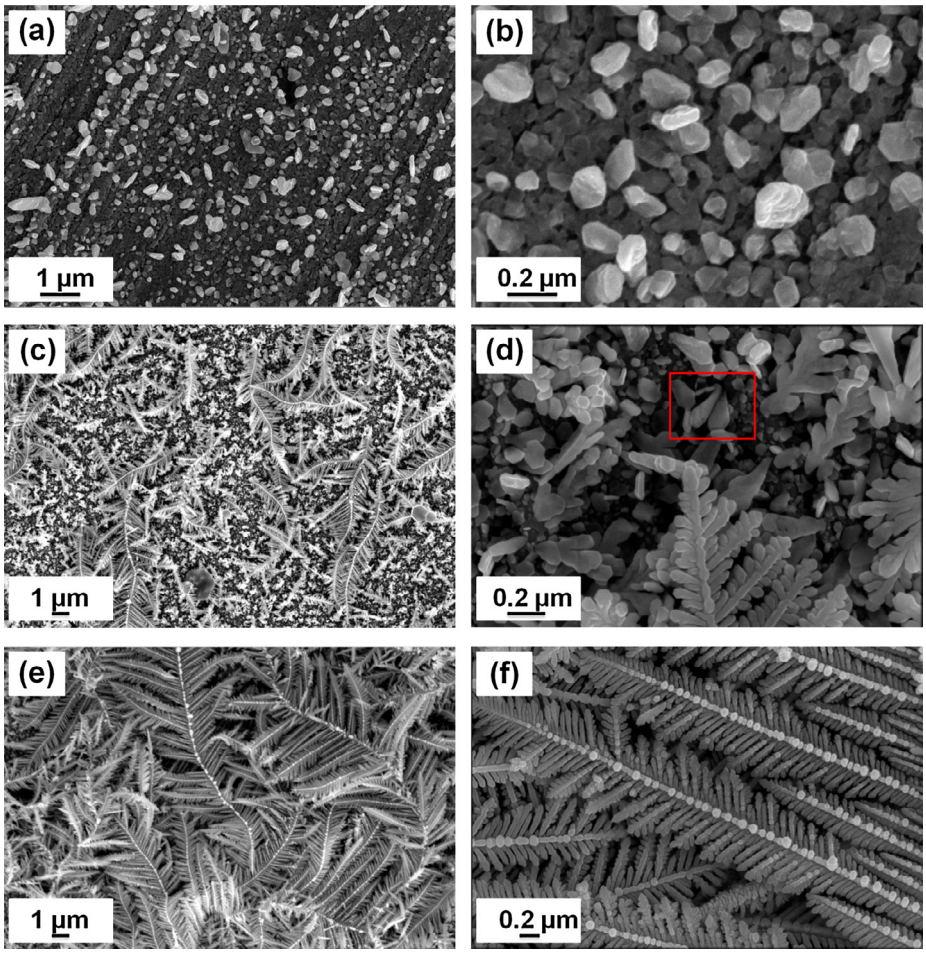

Fig. 1. Typical low (left column) and high (right column) magnification SEM images of Ag-Cu substrate with different reaction time of 4 min (a, b), 8 min (c, d), and 20 min (e, f), respectively.

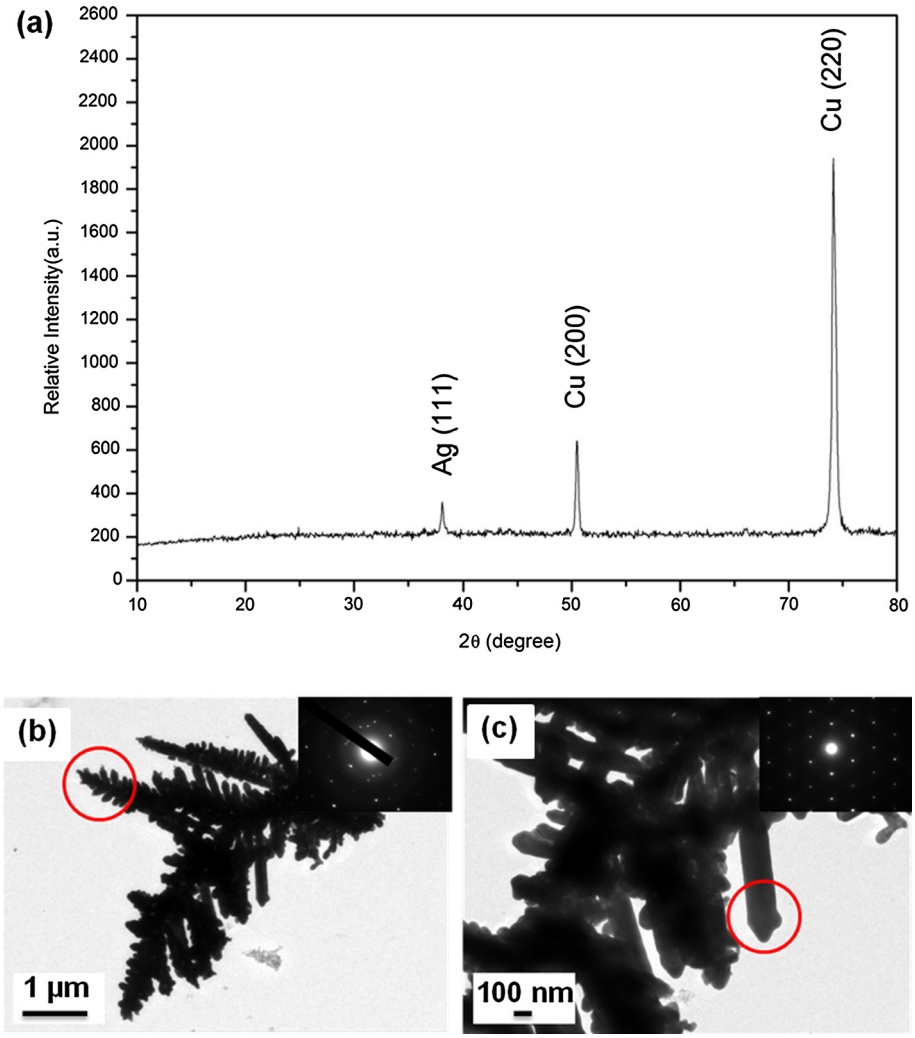

Fig. 2. (a) XRD pattern and (b, c) typical TEM images of Ag-Cu substrate with the reaction time of 20 min. Insets are the SAED patterns of the marked areas in (b) and (c), respectively.

the $AgNO_3$ aqueous solution with a concentration of 3.33 mM was used to react with Cu foils at room temperature. The reaction time was controlled to be 1, 2, 4, 8, 12, and 20 min, respectively. The final Ag-Cu substrates were rinsed with DI water and then used for SERS tests.

The surface morphologies of the Ag-Cu substrates were characterized using a scanning electron microscopy (SEM, Zeiss Gemini Ultra-55). Energy dispersive spectroscopy (EDS) in SEM was also used for elemental analysis. The crystalline quality of Ag-Cu substrates was investigated by X-ray diffraction (XRD, Bruker D8). Selected area electron diffraction (SAED) of the Ag nanostructures was further checked in a transmission electron microscopy (TEM, JEOL JEM-2100) at 200 kV. The SERS experiments were tested using a Raman spectrometer (Horiba HR-800) with an excitation laser working at 532 nm in wavelength.

3. Results and discussion

The surface morphologies of the Ag-Cu substrates were characterized by SEM. Fig. 1 presents typical SEM images of the Ag-Cu substrates prepared with different reaction time. Fig. 1(a) and (b) shows the observed morphologies of the Ag-Cu substrates with the reaction time of 4 min. A nanoparticle-aggregated fractal pattern is formed. A close look at the magnified image from Fig. 1(b) shows that the Ag nanoparticles demonstrate an isolated, sheet-like geometrical shape. As the reaction time increases, the Ag nanoparticles form the seeds to facilitate the further growth of Ag nanostructures. Fig. 1(c) and (d) shows the morphologies of the grown nanostructures with the reaction time of 8 min. It can be seen that the dendritic Ag nanostructures appear, which makes the morphology a drastic difference from that observed in Fig. 1 (a) and (b). The marked area by the red line in Fig. 1(d) indicates the formed basic unit of Ag dendritic nanostructures. As the reaction time further increases, dendritic Ag nanostructures become much dense and thick. Fig. 1(e) and (f) demonstrates the observed typical morphologies of the grown nanostructures with the reaction time of 20 min. The stems and branches of dendrites become thicker and longer. Meanwhile, distinct sub-branches appear as well, forming a clear fractal pattern.

Table 1
Measured Ag/Cu atom ratios on the surface of copper foils for the dendritic Ag nanostructures with the reaction time of 4, 8, and 20 min, respectively.

Atom ratio	Reaction time		
	4 min	8 min	20 min
Ag	9.27%	28.13%	74.79%
Cu	90.73%	71.87%	25.21%

The crystalline quality of the Ag nanostructures was further investigated using X-ray diffraction. Fig. 2(a) is the measured XRD pattern for a Ag-Cu substrate with the reaction time of 20 min, indicating that the synthesis of Ag is of excellent crystallinity. The observed three diffraction peaks can be indexed to diffraction from the (111) of face-centered cubic Ag and the (200), (220) of face-centered cubic copper. A refined lattice parameter $a = 2.35896$ Å is extracted from the XRD data, which is in good agreement with the previous report [36]. It is noted that the Cu signal is much stronger than the Ag one from Fig. 2(a) since the main ingredient is copper in the Ag-Cu substrate. The crystalline quality of the Ag nanostructure can be also cross-checked through the SAED diffraction pattern in TEM. Fig. 2 (b) and (c) shows typical TEM images of the Ag dendrites prepared in $AgNO_3$ solution for 20 min. We can see that the tip of the Ag branch shows polycrystalline characteristic [the inset of Fig. 2 (b)], while the stem illustrates a single-crystal feature [the inset of Fig. 2(c)]. Both XRD and SAED results have confirmed excellent crystallinity of the dendritic Ag nanostructures.

As mentioned, the dendritic Ag nanostructures were grown on copper foils via galvanic replacement reaction. It is therefore expected that the Ag/Cu atom ratio at the interface will change

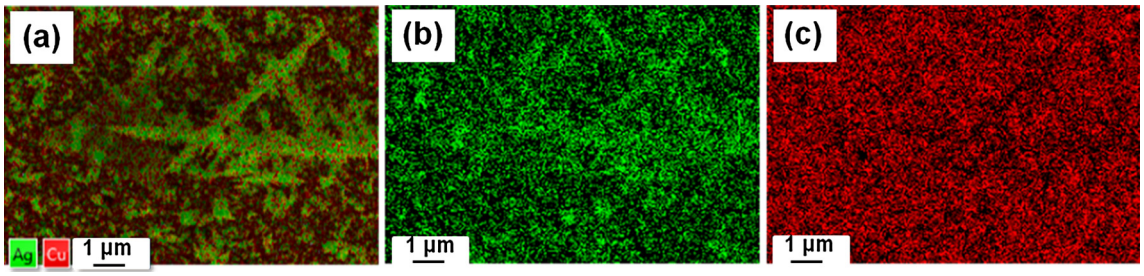

Fig. 3. Surface mapping of the dendritic Ag nanostructures with the reaction time of 20 min.

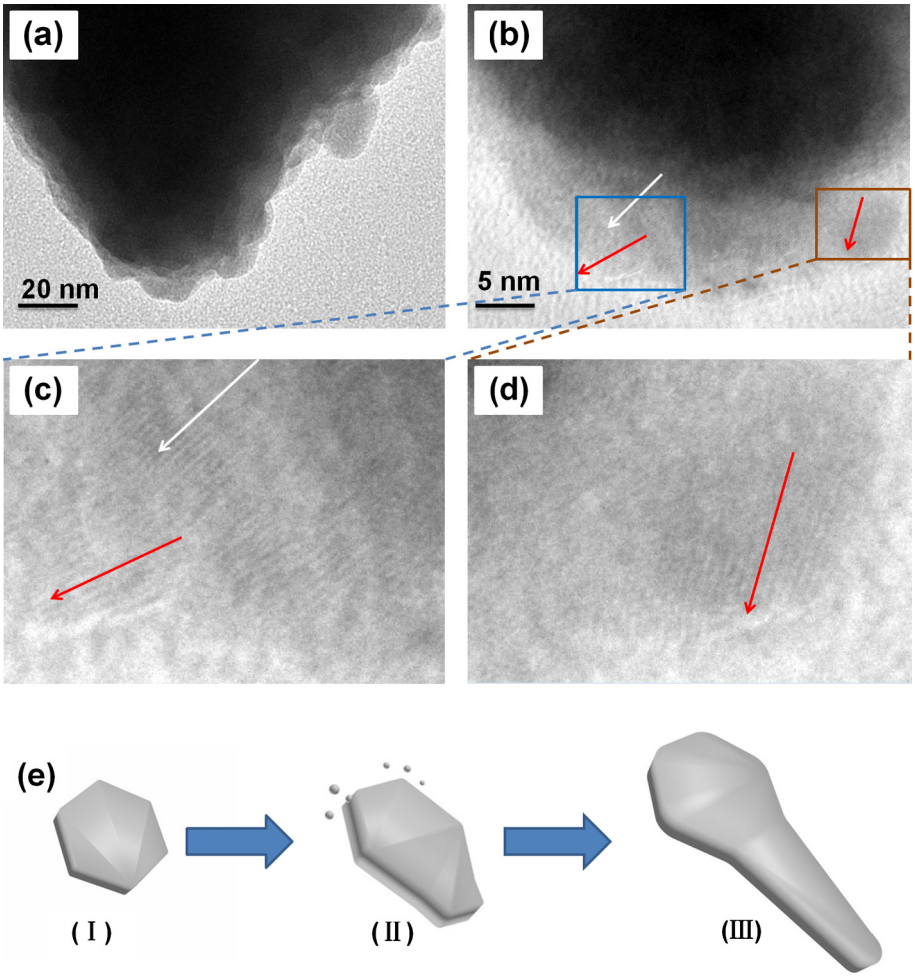

Fig. 4. HRTEM images of Ag dendrites indicating the OR (a) and OA (b) crystal growth mechanisms. (c, d) Magnified parts as marked in (b). Arrows in (b, c, and d) indicate the crystalline orientation. (e) Schematic representation of proposed morphological evolution for a basic unit in Ag dendrite growth: stage (I) seed formation of hexagonal Ag nanostructure; stage (II) simultaneous occurrence of OA-enabled orientation-preferred stretching and OR-enabled small nanocrystals adsorption; stage (III) formation of a basic unit in Ag dendrites.

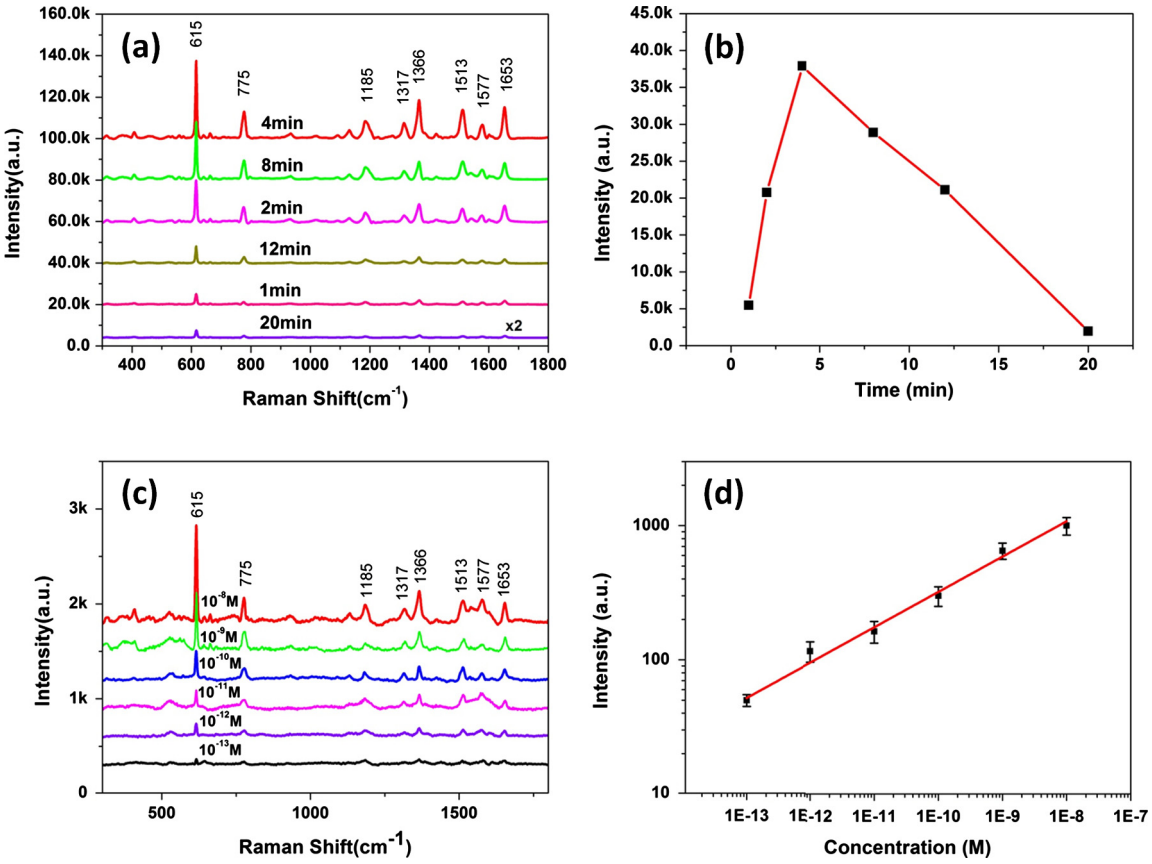

Fig. 5. (a) Raman spectra of R6G with a concentration of 10^{-5} M on different Ag-Cu substrates resulted from the reaction time of 1, 2, 4, 8, 12, and 20 min, respectively. (b) Raman intensity of R6G at 615 cm^{-1} as a function of reaction time. (c) Raman spectra of R6G with different concentrations from 10^{-8} down to 10^{-13} M for the Ag-Cu substrate with the reaction time of 4 min. (d) Raman intensity of R6G at 615 cm^{-1} as a function of concentration in log scale.

with the reaction time. The Ag/Cu atom ratios on the foil surface were estimated by EDS in SEM. Table 1 shows the measured Ag/Cu atom ratios with the reaction time of 4, 8, and 20 min, respectively. We can see that as the reaction time increases, the Ag concentration increases and the Cu concentration decreases correspondingly. Fig. 3 shows the surface mapping of the dendritic Ag nanostructures with the reaction time of 20 min. The green[1] color represents silver, and the red color represents copper. As can be seen, the distributions of silver and copper are quite uniform.

Based on the above morphological observations, we herein propose a possible growth process for the Ag nanostructures evolution. At the beginning point, silver ions in the solution are reduced to form isolated solid nanoparticles. These nanoparticles will then serve as the seeds to grow continuously through the gradual deposition of atoms or ions on the copper surface, and finally develop into sheet-like geometrical shapes. In this process, OR will take the dominant role with diffusion being the main growth-controlling factor. Fig. 4(a) shows OR mechanism of Ag crystal growth: a small Ag crystallite starts to condense on the surface of a large crystallite governed by minimization of surface free energy. At a certain growth stage, OA growth mechanism occurs and gradually dominates the growing process. Fig. 4(b) shows the OA growth mechanism: the white arrow labels internal orientation of Ag crystal and the red arrow represents the orientation of Ag crystal at the edge. It seems that the silver nanocrystals are attached more or less along the ⟨111⟩ direction with a slight misorientation angle between them. These nanocrystals may then realign themselves with respect to each other to grow along a common direction during the further growth. The above proposed growth process can be illustrated by a schematic diagram, as shown in Fig. 4(e). At the early stages of galvanic replacement reaction, the Ag nanostructure is Ag nanoparticles with relatively small anisotropy. The nanoparticles have a tendency to form sheet-like geometrical shape, as stage (I) shown in Fig. 4(e). Stage (II) indicates that a surface of the Ag nanostructure with both orientation-preferred stretching via OA growth mechanism and small nanocrystals adsorbed onto the surface of the nanostructure by OR mechanism, respectively. Stage (III) in Fig. 4(e) shows the formed basic unit of Ag dendritic nanostructures with its morphology similar to the observed one in Fig. 1(d). It is worth mentioning that, although there has been a great deal of discussion about the growth mechanism of similar nanostructures [37–39], it is still very challenging to describe the exact kinetics of the formation process of the dendritic Ag nanostructures. Our proposed model may only give an intuitive picture about the growth. We believe that the growth process involves both OR and OA mechanisms. These two mechanisms combine together and collectively contribute to the formation of the final Ag nanostructures.

Such Ag nanostructures have big potential for SERS sensing applications. To test their SERS sensitivity, rhodamine 6G (R6G) was chosen to experimentally characterize our Ag-Cu substrates. Fig. 5(a) shows the Raman intensities of R6G molecules with a concentration of 1×10^{-5} M, and the tested substrates were made by immersing Cu foils into 3.33 mM $AgNO_3$ with the reaction time of 1, 2, 4, 8, 12, and 20 min, respectively. To facilitate comparison and observation, Raman spectra were smoothened. The observed Raman peaks at 615, 775, 1185, 1317, 1366, 1513, 1577 and

[1] For interpretation of color in Fig. 3, the reader is referred to the web version of this article.

1653 cm^{-1} are all associated with the vibrational modes of R6G molecules, which agree well with the previous reports [40,41]. Fig. 5(b) describes the Raman intensity of R6G at the peak position of 615 cm^{-1} as a function of reaction time. From Fig. 5(a) and (b), it can be clearly seen that, as the reaction time increases, the Raman enhancement first increases and then decreases. It is well known that SERS effect is highly dependent on the number of "hot spots" produced by the noble metallic nanostructures. With short reaction time, Ag nanostructures (i.e., Ag nanoparticles) are small and sparse, and the interval between neighboring nanoparticles is big. As a result, the Ag nanostructures cannot provide massive "hot spots", making the Raman enhancement weak. While with too long reaction time, Ag nanostructures (i.e., Ag dendrites) become big and dense. The surface plasmons of the Ag dendrites might not be excited efficiently. Hence, there are not sufficient "hot spots" to enhance the SERS signal. Therefore, there is an optimum reaction time to grow the Ag nanostructure that can provide the maximum number of "hot spots" to produce the strongest SERS signal. From Fig. 5(b), we can see that the Raman enhancement is the strongest at the reaction time of 4 min, and the characteristic peak intensity at 615 cm^{-1} is approximately 40,000. Once we found the Ag-Cu substrate with the optimum SERS signal enhancement, we then used it to further test the detection limit. Fig. 5(c) shows the SERS spectra of R6G with different concentrations adsorbed on the Ag-Cu substrate with the reaction time of 4 min. It reveals that Raman spectral feature of R6G is clearly recognized and the SERS signal intensity increases with the increase of R6G concentration. Even when the R6G concentration is down to 10^{-13} M, the R6G Raman characteristic bands can be still obviously identified. The peak at 615 cm^{-1} was selected to investigate the relationship between Raman intensity and concentrations, as shown in Fig. 5(d). We can see an excellent linear response can be achieved, which will be highly useful to quantitatively calculate the concentration of the detection analyte using SERS.

4. Conclusions

In summary, we have demonstrated facile and low-cost fabrication of highly sensitive SERS substrates via replacement reaction. Different morphologies of Ag nanostructures were observed on the substrate surface by controlling the reaction time. We used combined OR and OA growth mechanisms to describe the formation process of dendritic Ag nanostructures on the Cu substrates. The Ag-Cu substrates showed optimum SERS enhancement at the reaction time of 4 min, and the minimum detected concentration of Rhodamine 6G was as low as 10^{-13} M. Our fabrication approach can produce well-defined Ag nanostructures with tailorable optical responses. The easy, low-cost fabrication and tailorable optical responses make the Ag-Cu SERS substrates promising for rapid, sensitive detection of targeted analytes.

Acknowledgments

The authors are grateful for financial support from the National Natural Science Foundation of China (11674199, 11604040, 11474187, 11404193), Excellent Young Scholars Research Fund of Shandong Normal University Shandong Province Natural Science Foundation (ZR2014FQ032, ZR2013EMM009, ZR2013HQ064).

References

[1] B. Sharma, R.R. Frontiera, A.I. Henry, E. Ringe, R.P.V. Duyne, Mater. Today 15 (2012) 16–25.
[2] M. Fleischmann, P.J. Hendra, A.J. McQuillan, Chem. Phys. Lett. 26 (1974) 163–166.
[3] M.G. Albrecht, J.A. Creighton, J. Am. Chem. Soc. 99 (1977) 5215–5217.
[4] D.L. Jeanmaire, R.P. Van Duyne, J. Electroanal. Chem. 84 (1977) 1–20.
[5] W.E. Doering, M.E. Piotti, M.J. Natan, Adv. Mater. 19 (2007) 3100–3108.
[6] R.M. Jarvis, R. Goodacre, Chem. Soc. Rev. 37 (2008) 931–936.
[7] X.M. Qian, S.M. Nie, Chem. Soc. Rev. 37 (2008) 912–920.
[8] K.W. Adu, M.D. Williams, M. Reber, R. Jayasingha, H.R. Gutierrez, G.U. Sumanasekera, J. Nanotechnol. 2012 (2012) 264198.
[9] W. Xie, P. Qiu, C. Mao, J. Mater. Chem. 21 (2011) 5190–5202.
[10] H.W. Qiu, S.C. Xu, P.X. Chen, S.S. Gao, Z. Li, C. Zhang, S.Z. Jiang, M. Liu, H.S. Li, D. J. Feng, Appl. Surf. Sci. 332 (2015) 614–619.
[11] P.X. Chen, S.B. Shang, L.T. Hu, X.Y. Liu, H.W. Qiu, C.H. Li, Y.Y. Huo, S.Z. Jiang, C. Yang, Chem. Phys. Lett. 660 (2016) 169–175.
[12] P. Hildebrandt, M. Stockburger, J. Phys. Chem. 88 (1984) 5935–5944.
[13] J.R. Lombardi, R.L. Birke, J. Phys. Chem. C 112 (2008) 5605–5617.
[14] V.I. Kukushkin, A.B. Van'Kov, I.V. Kukushkin, JETP Lett. 98 (2013) 64–69.
[15] S.A. Maier, Plasmonics: Fundamentals and Applications, Springer, New York, 2007.
[16] M.S. Wang, C.L. Zhao, X.Y. Miao, Y.H. Zhao, J. Rufo, Y.J. Liu, T.J. Huang, Y.B. Zheng, Small 11 (2015) 4423–4444.
[17] K. Chen, E.S.P. Leong, M. Rukavina, T. Nagao, Y.J. Liu, Y.B. Zheng, Nanophotonics 4 (2015) 186–197.
[18] M.L. Seol, J.H. Kim, T. Kang, H. Im, S. Kim, B. Kim, Y.K. Choi, Nanotechnology 22 (2011) 235303.
[19] S. Nie, S.R. Emory, Science 275 (1997) 1102–1106.
[20] X.M. Lin, Y. Cui, Y.H. Xu, B. Ren, Z.Q. Tian, Anal. Bioanal. Chem. 394 (2009) 1729–1745.
[21] B. Ren, G.K. Liu, X.B. Lian, Z.L. Yang, Z.Q. Tian, Anal. Bioanal. Chem. 388 (2007) 29–45.
[22] L. Wang, H.L. Li, J.Q. Tian, X.P. Sun, ACS Appl. Mater. Interfaces 2 (2010) 2987–2991.
[23] S. Lal, N.K. Grady, J. Kundu, C.S. Levin, J.B. Lassiter, N.J. Halas, Chem. Soc. Rev. 37 (2008) 898–911.
[24] G. Sinha, L.E. Depero, I. Alessandri, ACS Appl. Mater. Interfaces 3 (2011) 2557–2563.
[25] F.L. Yap, P. Thoniyot, S. Krishnan, S. Krishnamoorthy, ACS Nano 6 (2012) 2056–2070.
[26] B. Sharma, M.F. Cardinal, S.L. Kleinman, N.G. Greeneltch, R.R. Frontiera, M.G. Blaber, G.C. Schatz, R.P. Van Duyne, MRS Bull. 38 (2013) 615–624.
[27] Q. Zhang, Y.H. Lee, I.Y. Phang, C.K. Lee, X.Y. Ling, Small 10 (2014) 2703–2711.
[28] J.F. Betz, W.Y. Wei, Y. Cheng, I.M. White, G.W. Rubloff, Phys. Chem. Chem. Phys. 16 (2014) 2224–2239.
[29] Y.F. Chan, C.X. Zhang, Z.L. Wu, D.M. Zhao, W. Wang, H.J. Xu, X.M. Sun, Appl. Phys. Lett. 102 (2013) 183118.
[30] C.-Y. Zhang, Y. Lu, B. Zhao, Y.-W. Hao, Y.Q. Liu, Appl. Surf. Sci. 377 (2016) 167–173.
[31] A. Gutes, R. Maboudian, C. Carraro, Langmuir 28 (2012) 17846–17850.
[32] C.B. Murray, D.J. Norris, M.G. Bawendi, J. Am. Chem. Soc. 115 (1993) 8706–8715.
[33] Y. Cheng, Y. Wang, D. Chen, F. Bao, J. Phys. Chem. B 109 (2005) 794–798.
[34] R.L. Penn, J.F. Banfield, Science 281 (1998) 969–971.
[35] E.J.H. Lee, C. Ribeiro, E. Longo, E.R. Leite, J. Phys. Chem. B 109 (2005) 20842–20846.
[36] J. Fang, H. You, P. Kong, Y. Yi, X. Song, B. Ding, Cryst. Growth Des. 7 (2007) 864–867.
[37] X. Wen, Y.-T. Xie, M.W.C. Mak, K.Y. Cheung, X.-Y. Li, R. Renneberg, S. Yang, Langmuir 22 (2006) 4836–4842.
[38] H. Liang, H. Zhao, D. Rossouw, W. Wang, H. Xu, G.A. Botton, D. Ma, Chem. Mater. 24 (2012) 2339–2346.
[39] Y. Wang, S.-I. Choi, X. Zhao, S. Xie, H.-C. Peng, M. Chi, C.Z. Huang, Y. Xia, Adv. Funct. Mater. 24 (2014) 131–139.
[40] Y.K. Kim, S.W. Han, D.H. Min, ACS Appl. Mater. Interfaces 4 (2012) 6545–6551.
[41] S.C. Xu, S.Z. Jiang, G.D. Hu, J. Wei, L. Wang, J.Y. Zhang, Q.J. Li, Laser. Phys. 25 (2015) 115601.